Effect of O-vacancy concentration and proximity on the electronic metal-support interactions: Ru/ZrO_2 catalysts

Mengru Li, Axel Groß and R. Jürgen Behm*

Institute of Theoretical Chemistry, Ulm University,

Albert-Einstein-Allee 11, D-89081 Ulm, Germany

Abstract

Continuing our investigation of electronic metal-support interactions (EMSIs) in heterogeneous catalysis, we have investigated the effect of an increasing number of oxygen vacancies at the Ru-ZrO_2 interface of supported Ru/ZrO_2 catalysts on the CO adsorption properties. Employing density functional theory based calculations and using a model system consisting of a $ZrO_2(111)$ support and a Ru nanorod, we determined and discuss trends in the O-vacancy formation energy, in the interaction and charge transfer between support and Ru nanorod, in the local density of states on the Ru adsorption sites, in the CO adsorption energy and in the C-O vibrational frequencies as a function of an increasing number of oxygen vacancies at the Ru-ZrO_2 interface. Finally, we address consequences for our understanding of the role of EMSIs in heterogeneous catalysis and implications for the catalytic performance of realistic catalysts supported on reducible oxides.

Keywords: Catalysis, adsorption, electronic metal-support interactions, DFT calculations, Ru, ZrO_2, CO

Submitted to ACS Catal.: 06.05.2022

* Corresponding author, email juergen.behm@uni-ulm.de

1 Introduction

Metal-support interactions (MSIs), i.e., interactions between a support and an active metal phase, are well known to often decisively affect the performance of supported metal nanoparticle (NP) catalysts.[1-5] These include both structural effects, e.g., by partial overgrowth of the metal nanoparticles by a thin layer of the partly reduced oxide support material, the so-called classical strong metal-support interaction,[1;2] and electronic effects, induced by charge transfer between support and active metal NPs (electronic metal-support interactions – EMSIs).[3;6] Separation of these two different fundamental effects, however, is often cumbersome or even impossible, as in many or even most cases they both occur concurrently. Furthermore, contributions from these effects may sensitively depend on genuine catalyst properties such as size and shape of the metal NPs and on the reaction conditions. Considering electronic metal support interactions, it is furthermore unclear whether these affect the entire nanoparticle, as commonly indicated in the catalysis literature ('charge transfer to the metal nanoparticle'), or whether the charge transfer and the related modifications in the chemical properties are locally confined, as indicated in more recent theoretical studies.[7;8] For the former case one would expect a continuous change in the chemical / catalytic properties with increasing number of O-vacancies, while in the latter case modified and non-modified sites are expected to coexist.

Recently, we have reported on the influence of O-vacancies on the CO_2 methanation reaction at Ru/ZrO_2 catalysts and could demonstrate that their presence can significantly modify the catalyst performance in this reaction.[9] In particular, they affect the selectivity for methane formation ('CO_2 methanation') or, alternatively, for the formation of CO via the reverse water gas shift (RWGS) reaction. This catalyst system is particularly suited for model studies of metal-support interactions as structural modifications of the catalyst could be excluded under the conditions used in that study.[9] Accordingly, the observed changes in reaction performance

are solely caused by changes in the electronic properties of the Ru nanoparticles, due to electronic metal-support interactions. The changes in the electronic properties of different Ru sites in the Ru nanoparticle were tested by density functional theory (DFT) based calculations. Using a Ru nanorod supported on a ZrO_2(111) substrate as a model, we could demonstrate that the presence of an O-vacancy at the interface can lead to a significant modification of the local charge on the Ru atoms and a corresponding increase in the CO adsorption energy, if the Ru atom is in close proximity to the O vacancy. This means that mainly interface Ru atoms were affected.

In that previous study we focused on the changes in the electronic and chemical properties introduced by a single O-vacancy, without considering that under reaction condition also more than one O-vacancy may be present, depending on the reductive character of the reaction gas mixture and a possible pre-treatment of the catalyst. In fact, there is ample of evidence for such kind of accumulation of O-vacancies underneath the active metal during reaction in reductive gas mixtures, e,g., during methanol synthesis from CO_2 and H_2 over supported Au/ZnO catalysts.[10;11] Even for CO oxidation over Au catalysts supported on reducible oxides such as TiO_2 it was demonstrated that exposure to a stoichiometric CO / O_2 gas mixture leads to the formation of lattice oxygen vacancies (O-vacancies) at the perimeter of the Au nanoparticles,[12;13] and to the formation of negatively charged $Au^{\delta-}$ sites.[14;15] where more than one O-vacancy per nanoparticle is expected to form. Finally, our previous work also demonstrated that O-vacancies can be formed on ZrO_2 underneath Ru nanoparticles during the CO_2 methanation reaction, under reaction conditions.[9] Most likely this occurs by reaction at the interface perimeter sites, where the Ru nanoparticle reduces the barrier for surface lattice oxygen removal,[16;17] and subsequent migration of the resulting O-vacancy to the region underneath the Ru nanoparticle.

For a better understanding of the effect of O-vacancy accumulation and the related charge transfer on the reactivity and adsorption properties of a supported catalyst, and specifically of a Ru/ZrO_2 catalyst, we now systematically explored the effect of an increasing number of O-vacancies at interface sites on the electronic and chemical properties of different Ru sites and on the CO adsorption behavior on these sites, using the same Ru nanorod model as employed previously.[9] Since we had shown previously that the energy for O-vacancy formation is by more than 2 eV lower for lattice oxygen species in contact with the Ru nanorod, we here only considered such sites. We calculate the energy for vacancy formation, the charge transfer between support and Ru nanorod and the interaction energy between the Ru nanorod and the $ZrO_2(111)$ support for an increasing number of O-vacancies at the interface (section 3.1). Next, we determine the CO adsorption energies and preferable CO adsorption sites at four different representative locations of the Ru nanorod, as well as the total charge transfer to the adsorbed CO (section 3.2). For comparison with trends expected from the d-band model,[18] we also determine the center of the d-band on the respective adsorption sites and also calculate the frequencies of the C-O stretch vibration. For a more fundamental understanding of the underlying physical effects, we also determine the LDOS of the 4d-states of the Ru atoms binding to CO and of the π-states of CO for the different adsorption sites as a function of O-vacancy concentration (section 3.2). To identify synergistic effects of the support and the Ru nanorod in the CO adsorption properties we furthermore evaluate contributions from different regions in the Ru nanorod and from the support to the charge transfer to the adsorbing CO (section 3.3). Finally, we discuss consequences of our findings for our understanding of the role of EMSIs in heterogeneous catalysis and implications for the catalytic performance of realistic catalysts supported by reducible oxides (section 3.4).

2 Computational details

Spin-polarized periodical DFT calculations were performed using the Vienna ab initio software package (VASP) [19-21] with ionic cores described by the projected augmented wave (PAW) method.[22;23] The Perdew-Burke-Ernzerhof (PBE) functional [24] was used to describe exchange-correlation effects within the generalized gradient approximation (GGA). The cut-off energy of the plane wave basis in the expansion of the wave functions was set to be 600 eV. On-site Coulomb interactions were considered using the DFT+U approach [25;26] to treat the highly localized 4d states of Zr. The parameter U-J = 4.00 eV was taken from a previous work.[27] Dispersion corrections were taken into account within the DFT-D3 method.[28] At room temperature, the most stable bulk ZrO_2 phase is γ-monoclinic ZrO_2, which was also used in this work. A k-point mesh of 9 × 9 × 9 [29] was employed to determine the bulk structure of γ-monoclinic ZrO_2. Ionic bulk relaxations were supposed to reach convergence for forces below 0.001 eV/Å. The Ru/ZrO_2(111) model from our previous work [9] was used, in which a three-layer nanorod with a (3 × 3) super cell of Ru(0001) was placed on the (1 × 3) super cell of ZrO_2(111). The bottom six layers of ZrO_2 were fixed, and we relaxed the Ru atoms and the uppermost three layers of the ZrO_2(111) support. The k-point mesh was set to be 3 × 3 × 1 for the Ru_x/ZrO_2 slabs, due to the observed negligible energy variation between 5 × 5 × 1 and 3 × 3 × 1 meshes for the (1 × 3) super cell of ZrO_2(111). Finally, we used the charge partitioning method reported by Manz et al. [30;31] to calculate charges. This method is well-suited for strongly polarized systems.[32] Still, we tested this approach against other charge partition schemes, which yielded the same trends as far as changes and differences in the charge states are concerned.

The clean Ru/ZrO_2 and Ru/ZrO_{2-x} models with one O-vacancy were taken from our previous work, using a ZrO_2(111) support and a 3-layer [$11\bar{2}0$] oriented Ru nanorod (see Figure 1).[9] Additional O-vacancies close to the CO adsorption site were created by removing up to 4 adjacent surface lattice O-atoms, forming an O-vacancy cluster with up to 5 oxygen vacancies.

All of the O-vacancies were in contact with the Ru nanorod. The resulting model catalysts are denoted as 0 V_O, 1 V_O, 2 V_O, 3 V_O, 5 V_O; a structural model is presented in Figure 1. This model also shows the positions of the O-vacancies relative to the Ru nanorod. Since this work focuses on clarifying local effects of O-vacancies on CO adsorption, the first three O-vacancies are located along the edge of the Ru nanorod in the $[11\bar{2}0]$ direction. The fourth and fifth O-vacancies are created closer to the center of the Ru nanorod.

The interaction strength between the Ru slab and the support per contact area is evaluated using the equation

$$E_{interaction} = (E_{Ru\text{-}ZrO2\text{-}x} - E_{Ru} - E_{ZrO2\text{-}x})/A \quad (1)$$

where x denotes the number of O-vacancies, and $E_{Ru\text{-}ZrO2\text{-}x}$, E_{Ru} and $E_{ZrO2\text{-}x}$ are the energies of the interacting Ru/ZrO_{2-x} system and of the isolated Ru nanorod and the ZrO_{2-x} support, respectively. A denotes the area covered by the Ru nanorod which equals 77.46 $Å^2$.

The energy for the formation of an (additional) O-vacancy, $E_{formation}$, for the bare support and the Ru/ZrO_2 model system, and the effect of the Ru nanorod on the vacancy formation energy, $E_{vac.stab.}$, were calculated using equations (2) – (4)

$$E_{formation,ZrO2}(x) = E_{ZrO2\text{-}(x)} - E_{ZrO2\text{-}(x\text{-}1)} - {}^1/_2\, E_{O2} \quad (2)$$

$$E_{formation,Ru/ZrO2}(x) = E_{Ru\text{-}ZrO2\text{-}(x)} - E_{Ru\text{-}ZrO2\text{-}(x\text{-}1)} - {}^1/_2\, E_{O2} \quad (3)$$

$$E_{vac.stab}(x) = E_{formation,Ru/ZrO2}(x) - E_{formation,ZrO2}(x) - ½\, E_{O2} \quad (4)$$

where x again denotes the number of O-vacancies, including the newly formed one, and E_{O2} refers to the total energy of the O_2 molecule.

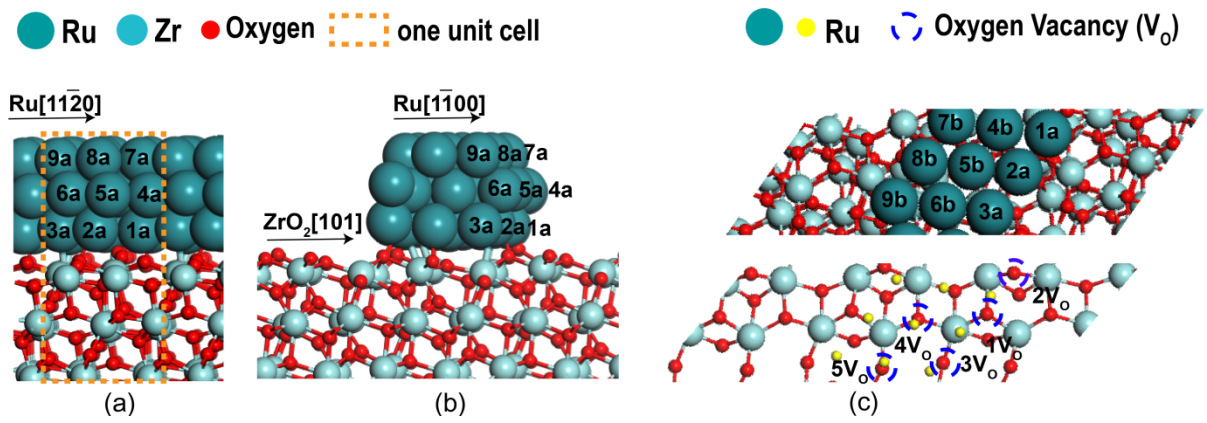

Figure 1 Side-views (a) and b)) and top-view (c) of the Ru/ZrO_2(111) model system including the location of the oxygen vacancies (lower panel).

3 Results and discussion

Before exploring the influence of O-vacancies on the CO adsorption properties, we first characterized the effect of the presence of the Ru nanorod on the energy required for the formation of O-vacancies at the interface and the effect of O-vacancies on the metal-support interaction and electron distributions at the interface. This will be followed by a systematic evaluation of the CO adsorption energies and sites. Finally the consequences of the O-vacancies on the binding of CO on these model systems with increasing concentration of O vacancies at the ZrO_2 / Ru interface will be addressed. Based on the Sabatier principle,[33] the adsorption energies should be directly related to the catalytic activity of Ru/ZrO_2 catalysts, e.g., for CO_2 methanation (see also ref. [9]).

3.1 Metal – Support Interaction

Vacancy formation energies: First, we calculated the energy required for the formation of an additional O vacancy for different sizes of the O-vacancy cluster according to equation (2), to learn about possible trends favoring the formation of vacancy clusters, both on the pristine ZrO_{2-x}(111) surface and underneath the Ru nanorod, as compared to dispersed individual O-vacancies. As reported already earlier,[9] the formation of a single O-vacancy requires 6.34 eV for the bare

ZrO_2(111) support, while underneath the Ru nanorod, this is reduced to 3.52 eV (for the same O-vacancy) (see Table S1). Hence, energetically the presence of the Ru nanorod significantly eases the formation of an O-vacancy as compared to a bare support by 2.82 eV in good agreement with experimental observations.[9] The energies required for the formation of additional, neighbored O-vacancies, in an increasing cluster of surface O-vacancies, are illustrated in Figure 2, both for the bare support (grey bars) and at the Ru-ZrO_2 interface (orange bars). While for the bare ZrO_2(111) the energies do not vary much with increasing number of vacancies, variations are quite substantial for the Ru/ZrO_2(111) model system. Therefore, for the bare ZrO_2(111) support interactions between neighboring vacancies are rather small. For the Ru/ZrO_2(111) model system, the vacancy formation energies are lowered to a different extent. The promotion caused by presence of the Ru nanorod strongly depends on the distance between the closest Ru atom and the surface O atom before its removal. For the first three O-vacancies underneath the edge of the Ru nanorod, with distances between the nearest Ru atom and the O-vacancy increasing from 2.13, 2.15 to 3.33 Å, the energy for the O-vacancy formation increases from 3.52 to 4.01 and 5.59 eV. In contrast, for the fourth and fifth vacancies $4V_O$ and $5V_O$, which are further away from the edge of the Ru nanorod, the O-vacancy formation energies are rather similar (4.24 eV and 4.29 eV). The higher energy required for the formation of the third O-vacancy ($3V_O$) results from its larger distance to the nearest Ru atom (Ru-3a). Obviously, the Ru nanorod promotes the O-vacancy formation of $1V_O$ and $2V_O$ close to its edge more strongly than of the vacancies below the center of the Ru nanorod ($4V_O$ and $5V_O$). For a more extended Ru/ZrO_2 catalyst this would mean that O-vacancies are preferentially generated at the edge of the Ru nanoparticle, at perimeter sites, and might then migrate further below the Ru nanoparticle upon the formation of new vacancies at the perimeter.

For a better understanding of the physical reasons leading to these pronounced variations in the O-vacancy formation energy we split the O-vacancy formation energy into two parts. The first part (pink bars in Figure 2) describes the O-vacancy formation energy on the bare ZrO_{2-x}(111) support, but using the respective optimum structures of the support obtained in contact with the Ru nanorod in the corresponding initial and final states for addition of an O-vacancy (frozen ZrO_{2-x}(111)). The second part (blue bars in Figure 2) accounts for the change in metal – support interaction when bringing the ZrO_{2-x} in their initial and final configurations (frozen ZrO_{2-x}, see above), respectively, into contact with the Ru nanorod. This process corresponds to the chemical interaction between support and Ru nanorod upon contact, without modifying their structure. Together, these two contributions yield the energy required for creating a O-vacancy in the Ru/ZrO_{2-x}(111) model system, where both initial and final state are fully relaxed

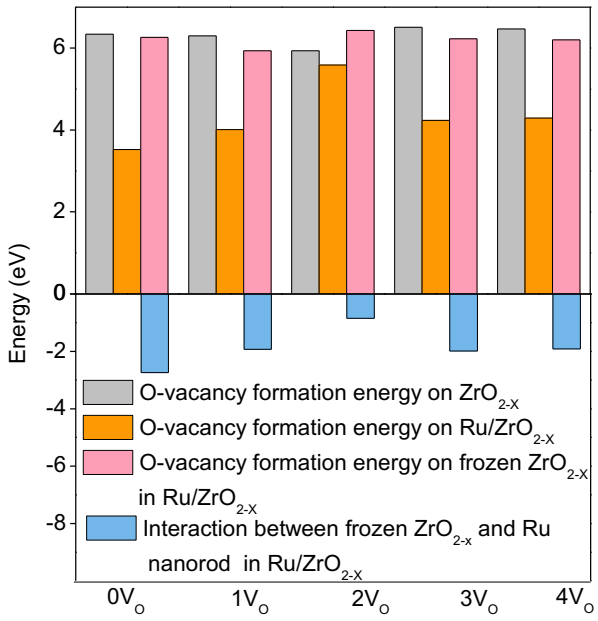

Figure 2 O-vacancy formation energy for an increasing number of vacancies on the bare, relaxed ZrO_{2-x}(111) (grey bars, see also Table S1), on the ZrO_{2-x}(111) using the frozen initial and final state structures obtained in contact with the Ru nanorod (pink bars), and on the relaxed Ru/ZrO_{2-x}(111) model system using relaxed initial and final states (orange bars, see also Table S1). Blue bars indicate the change in metal - support interaction energy when bringing the frozen ZrO_{2-x}(111) support (see text for explanation) into contact with the Ru nanorod. $0V_O$ etc. denote the surface before O-vacancy formation.

(see Table S1). The data in Figure 2 clearly demonstrate that it is mainly the second part, the change in metal – support interaction energy for the different ZrO_{2-x}(111) supports, which varies more significantly as a function of the number of vacancies. In contrast, the energy required for O-vacancy formation on the frozen ZrO_{2-x}(111) closely follows the behavior observed for O-vacancy formation on bare relaxed ZrO_{2-x}(111). Hence, the variation in the metal - support interaction for an increasing number of vacancies is the decisive contribution for the variation in the O-vacancy formation energy at the Ru – $ZrO_{2-x(}$111) interface.

Charge redistribution within the support and the Ru nanorod: For a more detailed picture of the changes in the surface and interface properties we furthermore evaluated the charge distribution at the surface of ZrO_{2-x}(111) and at the interface in the Ru/ZrO_{2-x}(111) model system, as well as the changes therein caused by the formation of O-vacancies. Before addressing these charge modifications, one should note that already the interaction with the Ru nanorod, i.e., the formation of the ZrO_2(111)–Ru interface, leads to a charge redistribution, namely a charge transfer from the ZrO_2(111) support to the Ru nanorod. This is illustrated in Figure 3, showing both the complete charge transfer from the support to the Ru nanorod and the partial charge transfer to the different layers of the nanorod. Clearly, this is dominated by the direct transfer to the Ru atoms in the interface layer (‘bottom layer’), while for the higher layers the charge transfer is much smaller. Exhibiting an oscillatory trend, the middle layer shows a slightly positive charge, and the top layer is again negatively charged, but to a very small extent. The resulting charges on the different Zr surface and interface ions and on the different Ru atoms are listed in Tables 1 and 2, respectively ($0V_O$). The numbering of the relevant Zr surface/interface ions and of the Ru atoms is illustrated schematically in Figure 4.

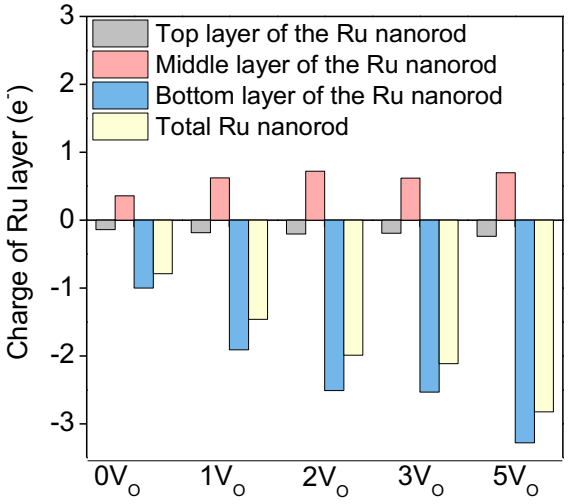

Figure 3 Charge transfer from the support to the Ru nanorod in total and to the top, middle and bottom layers of Ru atoms in the nanorod upon interaction of the Ru nanorod and the support as a function of the number of O-vacancies (increasing from 0 to 5).

In general, the formation of O-vacancies leads to the reduction of the neighboring Zr ions, resulting in partly reduced Zr^{n+} species. On the pristine $ZrO_2(111)$ surface, where one lattice oxygen coordinates to three Zr ions, the creation of a first oxygen vacancy ($1V_O$, Fig. 1c) mainly leads to a modification of the charge on the neighboring Zr ions. This is illustrated in Table 1, where the charge states of the relevant Zr ions are summarized, including the charge states in the fully oxidized surface. Here it should be noted that the charge on the Zr surface ions does not correspond to the formal value of 4+ because of surface effects and covalent contributions to the bonding. The same is true also for the O surface ions, where the calculated charge does not correspond to -2 e, but rather to -1.29 e. In the case of a single $1V_O$ vacancy the charge on the neighboring Zr ions 2Zr, 3Zr and 4Zr changes by 0.69 e (from +2.59 e to +1.90 e), 0.67 e (from +2.55 e to +1.88 e) and 0.69 e (from +2.59 e to +1.90 e), respectively (see Table 1), while the remaining Zr ions are only slightly reduced by 0.08 e. Interestingly and in contrast to expectations, also the neighboring oxygen ions are positively polarized by +0.84 e, which corresponds to about 0.1 e per O surface atom in contact with these reduced Zr ions. Hence, essentially the entire charge of the former $O^{1.29-}$ is transferred to the neighboring Zr and O ions.

Table 1 Above the table: Schematic representation of the surface and indication of the different Zr surface atoms and O-vacamcies (see also Figure 1 for comparison). In the table: Charges on the different Zr surface ions before and after formation of a single oxygen vacancy at the surface / interface in ZrO_{2-x}(111) and Ru/ZrO_{2-x}(111) model systems (unit: e).

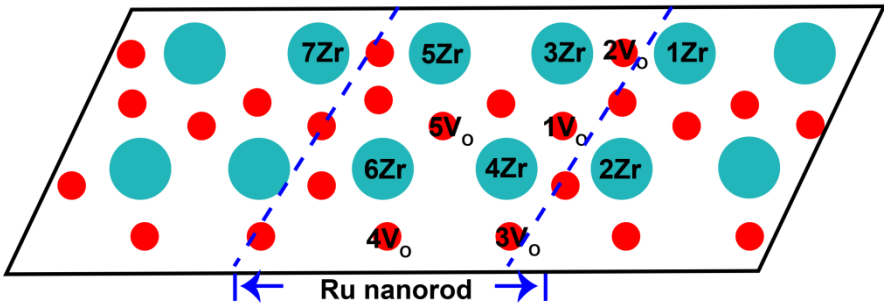

Zr atom	Without Ru nanorod					With Ru nanorod				
	0Vo	1Vo	2Vo	3Vo	5Vo	0Vo	1Vo	2Vo	3Vo	5Vo
1Zr	+2.56	+2.55	+1.76	+1.92	+1.83	+2.57	+2.55	+2.36	+2.31	+2.24
2Zr	+2.59	+1.90	+1.82	+1.88	+1.91	+2.55	+2.21	+2.20	+2.19	+2.19
3Zr	+2.55	+1.88	+1.22	+0.73	+0.53	+2.32	+2.03	+1.84	+1.38	+1.32
4Zr	+2.59	+1.90	+1.82	+1.13	+0.68	+2.35	+2.08	+2.08	+1.58	+1.36
5Zr	+2.56	+2.56	+2.54	+2.54	+1.30	+2.28	+2.29	+2.26	+2.20	+1.55
6Zr	+2.60	+2.59	+2.58	+2.55	+1.28	+2.34	+2.33	+2.32	+2.30	+1.67
7Zr	+2.55	+2.55	+2.56	+2.55	+2.54	+2.55	+2.54	+2.54	+2.54	+2.53

In the presence of the Ru nanorod, creating the same oxygen vacancy leads to less pronounced reduction of the neighboring Zr ions. Still, 0.34, 0.29 and 0.27 electrons are transferred to the Zr ion closest to the oxygen vacancy, leading to a decrease of the neighboring Zr ion charge from +2.55 e to +2.21 e, from +2.32 e to +2.03 e, and from +2.35 e to +2.08 e, respectively. In addition, 0.05 electrons are transferred to more distant Zr ions. The remaining charge is partly transferred to the Ru nanorod, whose total charge increases by 0.67 electrons upon 1Vo formation, from -0.79 e to -1.46 e (see Figure 3), while the other oxygen ions lose 0.62 e^-. This can be understood by an increased covalent contribution. The charging of the different Ru layers follows the trend in the fully oxidized case, namely that the charge transferred to the interface

layer exceeds the total charge transferred to the nanorod, while the central layer is slightly positively charged, followed by an even lower negative charge in the surface layer of the Ru nanorod. While the average electron density per Ru atom in the nanorod changes from 0.03 to 0.17 e, the average electron density per Ru atom in the interface layer increases from 0.11 to 0.36 e. Furthermore, there is an obvious distance dependence in the charge transfer, i.e., the closer to the O-vacancy, the more negatively charged the Ru atom (see Table 2). Upon O-vacancy formation, the Ru atom (Ru-1a), which is closest to the O-vacancy with a distance of 2.13 Å, is charged by -0.82 e (from +0.20 to -0.62 e). Charging changes by -0.25 e and +0.03 e for distances of 2.53 Å (Ru-2a) and 3.26 Å (Ru-4b), and by 0.06 e for a distance of 4.39 Å (Ru-4a) (see Table 2). Hence, for larger distances the changes in the Ru charge state become negligible.

Table 2 Charge on the Ru interface atoms (1a - 3a, 4b - 9b) and on the Ru atoms involved in CO binding (1a – 9a) on the $Ru/ZrO_{2-x}(111)$ model systems in the presence of 0 – 5 oxygen vacancies at the interface (unit: e). Numbering of the Ru atoms see Figure 1.

Ru atom	**Catalyst**				
	$0V_O$	$1V_O$	$2V_O$	$3V_O$	$5V_O$
1a	+0.20	-0.62	-1.02	-0.99	-1.04
2a	-0.24	-0.49	-0.48	-0.35	-0.16
3a	-0.19	-0.05	-0.40	-0.54	-0.51
4a	+0.06	+0.12	+0.05	-0.03	-0.17
5a	-0.10	+0.03	+0.10	+0.06	+0.04
6a	+0.00	+0.01	+0.02	+0.02	+0.01
7a	+0.00	-0.01	-0.01	+0.03	+0.06
8a	-0.01	-0.04	-0.04	-0.06	-0.06
9a	-0.04	-0.04	-0.04	-0.05	-0.07
4b	-0.41	-0.38	-0.33	-0.36	-0.25
5b	-0.13	-0.12	-0.07	-0.08	-0.71
6b	+0.04	+0.02	+0.05	+0.06	-0.54

7b	-0.08	-0.12	-0.10	-0.11	-0.01
8b	-0.10	-0.11	-0.12	-0.13	+0.03
9b	-0.08	-0.04	-0.05	-0.04	-0.11

Note: $0V_O$, $1V_O$, $2V_O$, $3V_O$ and $5V_O$ refer to a system with 0 – 5 oxygen vacancies

The formation of the second oxygen vacancy on the pristine ZrO_{2-x}(111) surface (model system $2V_O$ (Figure 1c)) further reduces the Zr^{n+} site in contact with both O-vacancies (3Zr) from +1.88 e to +1.22 e, and the site (1Zr) adjacent to the new O-vacancy is reduced from +2.55 e to +1.76 e, while there are little changes for the other Zr ions. In total, 1.45 electrons are transferred to the neighboring Zr ions, and 0.21 electrons to Zr ions more distant to the O-vacancy Zr ions. To compensate for the charge of the removed O-surface atom (1.18 e), also the charge on the (neighboring) O atoms changes by 0.48 e. In the presence of the Ru nanorod, the charge transfer to the neighboring Zr ions and hence their reduction is less pronounced, as already observed for the first O-vacancy formation. The charges on the Zr ions adjacent to the new vacancy, 3Zr and 1Zr, change from +2.55 e and +2.03 e to +2.36 e and +1.84 e. Hence, only 0.38 electrons are transferred to the Zr ions directly neighbored to the new oxygen vacancy. Another 0.53 electrons are transferred to the Ru nanorod after $2V_O$ formation, leaving the Ru nanorod with a negative charge of 1.99 e^- afterwards. Also in this case we find an oscillatory trend in the charge transfer to the different Ru layers, with a mean negative charge of 0.28 e on the interface atoms, whereas the Ru atoms directly neighboring the two O-vacancies are affected most.

Similar trends are also observed for the formation of the third and fifth oxygen vacancy ($3V_O$ and $5V_O$ in Figure 1c), as is evident from the charge distributions shown in Figure 3 and those listed in Tables 1 and 2. As shown in Figure 4a, this results in an essentially linear increase of the accumulated charge transfer to the Ru nanorod with increasing of O-vacancy concentration. The variations in the individual O-vacancy formation energies (Figure 3) are reflected by slight deviations from a linear fit. Again, most of the electrons transferred to the Ru nanorod are

localized at the interface, i.e., in the bottom layer of the Ru nanorod. Furthermore, the increased charge transferred from the support to the interface also lowers the reduction of the Zr ions neighboring theo O-vacancies. Overall, these data show a pronounced local confinement of the charge transfers induced by the O-vacancy formation, both vertically and laterally.

Metal – support interaction energies: Finally, to demonstrate the influence of the O-vacancies on the metal-support interaction, we calculated the mean interaction energies between the support and the Ru nanorod per interface area and its variation upon introducing an increasing number of O-vacancies. Because of the significant deformation of the epitaxial Ru structure, the interaction energy was calculated using the oxide support and the Ru nanorod of the strained structure taken in the $Ru/ZrO_{2-x}(111)$ system [9]. As illustrated in Figure 4b, the O-vacancies enhance the interaction strength between the Ru nanorod and the support. Note that this differs from the values given in Figure 2 (blue bars), as in the latter the frozen $ZrO_{2-x}(111)$ support was used as initial state. The mean interaction energy increases from -147.34 meV $Å^{-2}$ for the fully oxidized $ZrO_2(111)$ support without any vacancies to -289.90 meV $Å^{-2}$ for the $5V_O$ system. Actually, there is an almost linear relationship between the metal-support interaction and the number of oxygen vacancies (Figure 4b). This trend is consistent with the effect of metal-

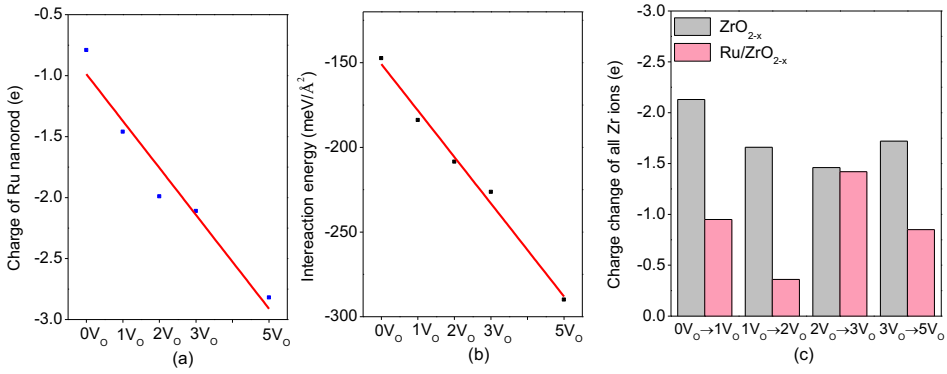

Figure 4 a) Charge on the entire Ru nanorod, b) mean interaction energy between the Ru nanorod and the support (structures see text) as a function of the number of O-vacancies, and c) total charge change of all Zr ions upon formation of an additional O-vacancy on ZrO_{2-x} and $Ru/ZrO_{2-x}(111)$ models.

support interactions on the O-vacancy formation process indicated by the blue bars in Figure 2, in agreement with the small variations in O-vacancy formation energies on the bare support. As shown in Figure 2, the Ru nanorod favors the O-vacancy formation process through the metal-support interaction, causing a charge transfer to the Ru nanorod. Figure 4c compares the change in the charge of the Zr ions (in the entire unit cell) upon O-vacancy formation in the absence (grey bar) and presence (pink bar) of the Ru nanorod. While for the bare ZrO_{2-x}(111) this charge transfer is between 1.5 and 2.1 e, the charge transfer to the Zr ions is by about 1 e per O-vacancy lower for the Ru/ZrO_{2-x}(111) system. Only for the third O-vacancy formation there is almost no difference between these two scenarios, which we attribute to the relatively larger distance between the oxygen atom to be removed and the closest interface Ru atom. These variations in the charge transfer are also responsible for the deviation of the data points from a purely linear relation in Figure 4a and also in Figure 4b. Generally, a higher number / density of O-vacancies leads to an increasing accumulated electron transfer from the support

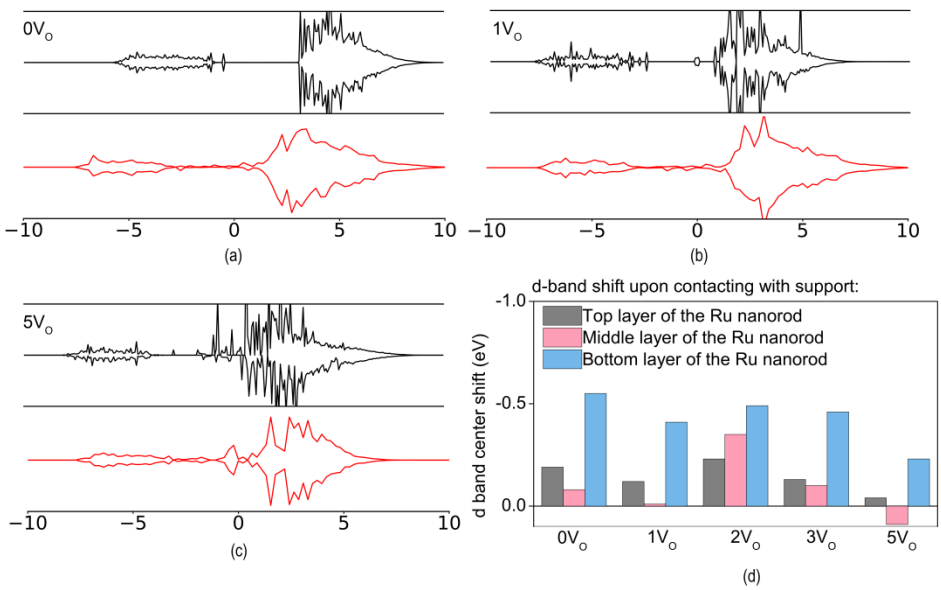

Figure 5 Local density of states of the 4d-band of the Zr ions underneath the Ru nanorod for $0V_O$ (a), $1V_O$ (b) and $5V_O$ (c) in the absence (black d) and in contact with (red) the Ru nanorod. (d) Shift of the 4d-band center of the Ru atoms in the top, middle and bottom layer of the Ru nanorod in contact with the support.

to the Ru nanorod (Figure 4a) and an enhanced metal-support interactions. In order to obtain more insights into the interaction between support and Ru nanorod, we evaluated the (averaged) local density of the 4d states of the Zr ions directly underneath the Ru nanorod, both for the pure ZrO_{2-x}(111) support and for the Ru/ZrO_{2-x}(111) model catalyst with 0, 1 and 5 O-vacancies ($0V_O$, $1V_O$, and $5V_O$, Figure 5a - 5c). For the $0V_O$ system, a mostly unoccupied broad d-band with its center well above the Fermi energy is visible for the pure ZrO_2(111) surface. After depositing the Ru nanorod, the band broadens significantly and shifts to lower energies, resulting in d-LDOS close to the Fermi level, as shown in Figure 5a. The presence of a single O-vacancy leads to a downshift of the Zr-4d LDOS for the free support, but the majority of the band still remains well above the Fermi energy. In contact with the Ru nanorod the band broadens, also increasing the portion of the LDOS below the Fermi level (Figure 5b). Finally, for the $5V_O$ system, there is significant of the LDOS below the Fermi level already for the free Ru/ZrO_{2-x}(111) support (Figure 5c), but also upon deposition of the Ru nanorod. Note that the Ru 4d-band within the nanorod is also affected by the interaction with the support. These changes are reflected in the shifts of the center of the 4d-band in the different Ru layers of the nanorod upon interaction with the ZrO_{2-x}(111) support, which are illustrated in Figure 5d as a function of the number of O-vacancies, from $0V_O$ to $5V_O$ see also Figure S1). In general, the center of the Ru 4d-band shifts to lower energies upon interaction with the support. This shift is most pronounced, with values of around -0.5 eV, for the Ru atoms in the lowest layer at the interface. Except for the $5V_O$ system, the shifts vary little as a function of the number of O-vacancies, by less than ±0.1 eV. Only for the $5V_O$ system the downshift is significantly reduced by about 0.25 eV (Figure 5d). As a result, we expect a stronger hybridization of the 4d-states of the Ru atoms in the interface layer with the Zr surface atoms upon increasing the concentration of O-vacancies, leading to a higher binding energy between support and metal, as shown in Figure 4b.

Thus, the physical reason for the stronger metal-support interaction with an increasing number of O-vacancies should be related to a combination of increased chemical bonding and increased electrostatic interactions. The former results from changes in the electronic structure of the Zr ions and Ru atoms at the interface, allowing more efficient hybridization between the 4d states of Zr^{n+} and the Ru interface ions/atoms. The latter arises from an increasing charge transfer from the support to the Ru nanorod, and in particular to its interface layer, which in turn leads to an attractive electrostatic interaction between the negatively charged Ru layer and the positively charged ZrO_2 surface layer, which becomes stronger with an increasing number of vacancies.

3.2 CO adsorption on the Ru nanorods

Using CO as a chemical probe, we investigated the adsorption properties of different sites and their variation in the presence of an increasing number of O-vacancies at the interface. For a comprehensive picture of the adsorption characteristics, we calculated not only the CO adsorption energy and determined the preferred adsorption site, but also evaluated the charge transfer to the adsorbed molecules and the vibrational frequencies of the CO_{ad} species. In this approach, we tested CO adsorption on four different sites, one at the Ru surface layer, one at the middle layer and two in the Ru interface region, which we consider as being representative for CO adsorption away from the interface / O-vacancies and close to them, respectively. For adsorption at the interface between bottom Ru layer and support, two favorable adsorption regions were tested, termed as region i and region ii, which consist of the Ru atoms 1a, 4a and. 5a and of 2a, 3a and 6a, respectively. The different adsorption sites are illustrated in Figures 6 – 9, the CO adsorption energies resulting for the different adsorption sites are plotted also as a function of the number of O-vacancies in Figure 10a.

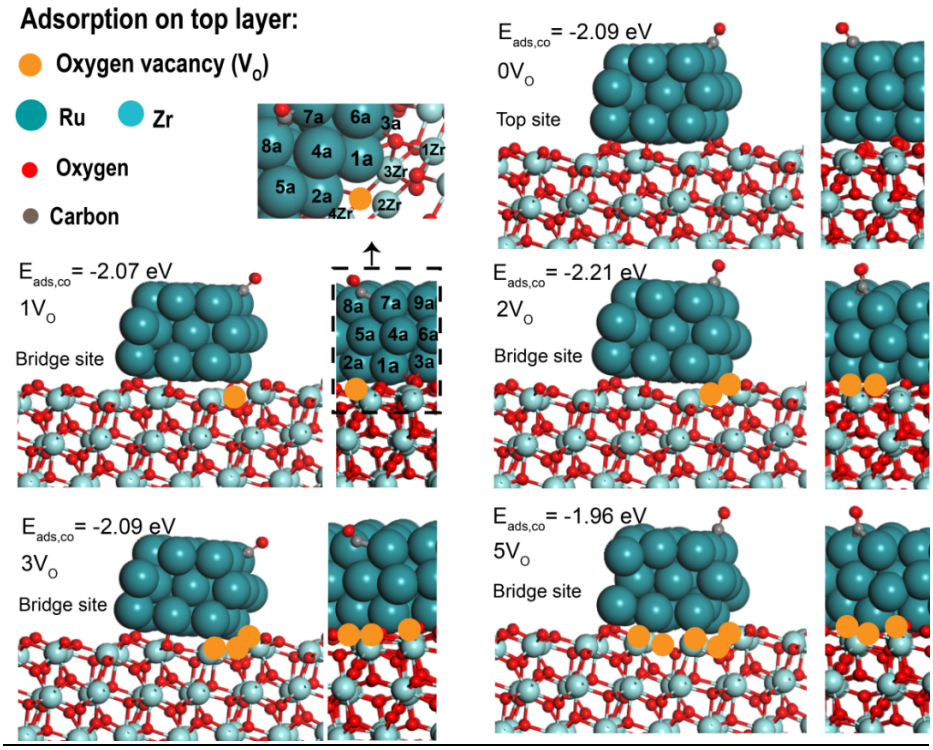

Figure 6 Side views illustrating the CO adsorption on the top layer of a 3-layer [11$\bar{2}$0] oriented Ru nanorod and the related adsorption energies in the presence of an increasing number of O-vacancies (0, 1, 2, 3, 5, see Figure) at the interface.

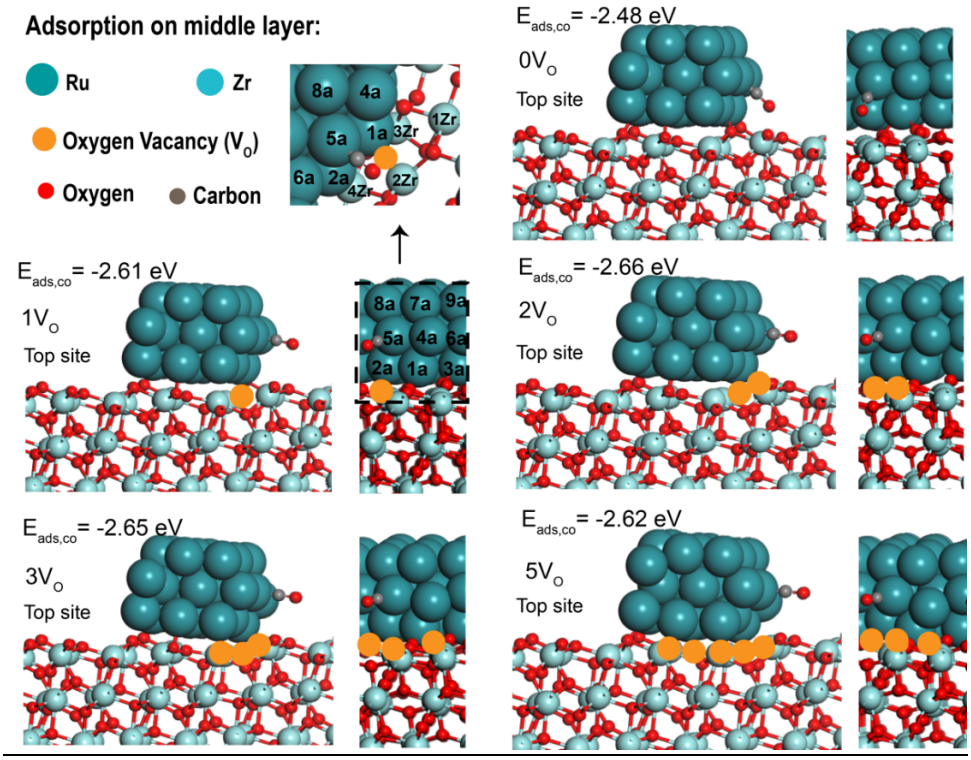

Figure 7 Side views illustrating the CO molecule adsorbed at middle layer of a 3-layer [11$\bar{2}$0] oriented Ru nanorod and the related adsorption energies in the presence of an increasing number of O-vacancies (0, 1, 2, 3, 5, see Figure) at the interface.

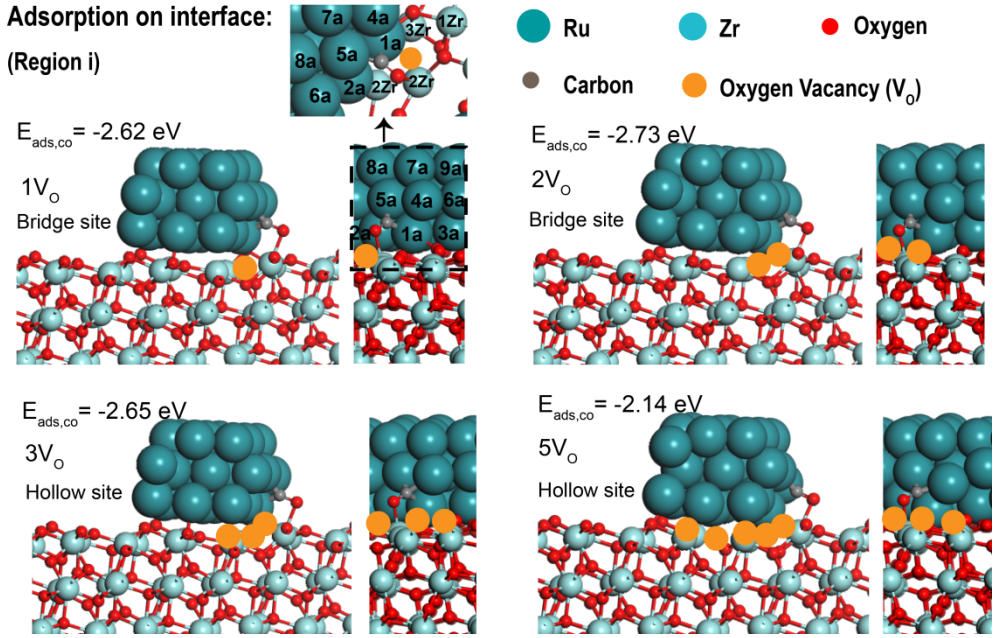

Figure 8 Side views illustrating the CO molecule adsorbed in the interface region i (Ru atoms 1a, 4a and 5a) of a 3-layer [11$\bar{2}$0] oriented Ru nanorod and the related adsorption energies in the presence of an increasing number of O-vacancies (0, 1, 2, 3, 5, see Figure) at the interface.

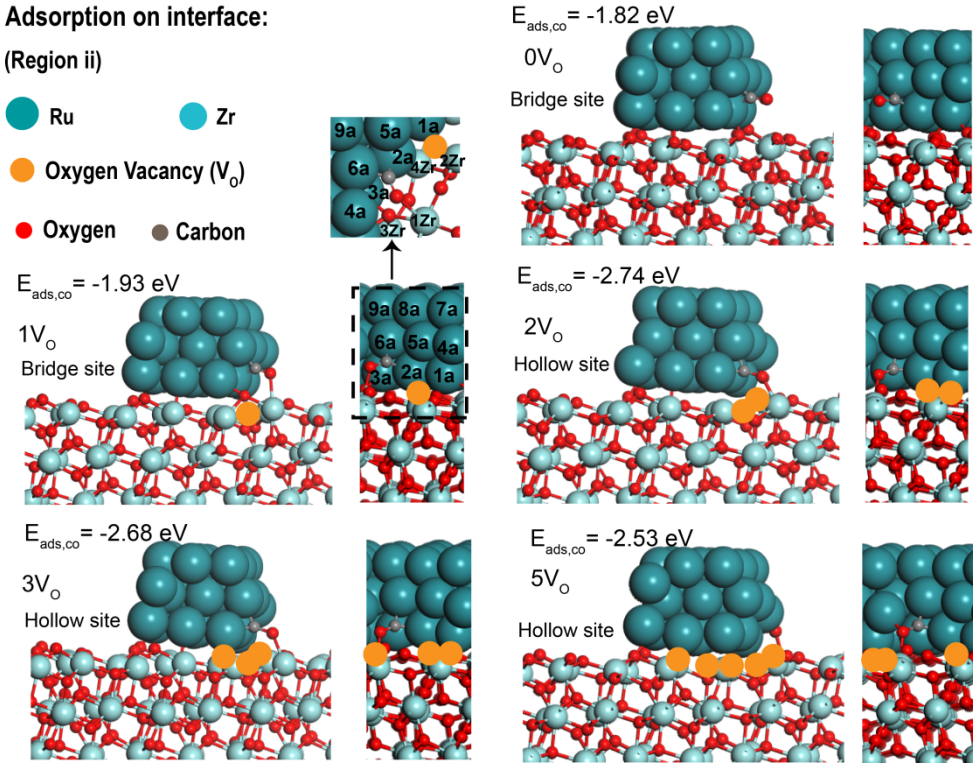

Figure 9 Side views illustrating the CO molecule adsorbed in the interface region ii (Ru atoms 2a, 3a and 6a) of a 3-layer [11$\bar{2}$0] oriented Ru nanorod and the related adsorption energies in the presence of an increasing number of O-vacancies (0, 1, 2, 3, 5, see Figure) at the interface.

Starting with the adsorption energy and the type of adsorption site occupied by CO, we had already shown in our previous work that there is a distinct difference in the adsorption energy at interface and surface different sites, both for the fully oxidized support and for the support with one O-vacancy at the interface.[9] For the fully oxidized support surface we obtained CO adsorption energies of -2.48 eV and -2.09 eV for adsorption on the interface site (region i) and on the surface site, respectively. [9] For adsorption on the top layer of the Ru nanorod (see Figure 6), we find preferential CO adsorption on an on-top site. Here it should be noted, that we would expect an even lower CO adsorption energy if the top-layer CO is located in the middle of the rod rather than at the edge, which in some cases was also confirmed by tests. Also for adsorption in the middle layer, we find preferential adsorption on an on-top site, on the 5a Ru atom (Figure 7). For adsorption at the metal-support interface (see Figures 8, 9), CO generally binds to one or more Ru atoms, involving also the interface layer, and a Zr ion at the support surface, forming Ru-C and O-Zr bonds. For the pristine support and adsorption in the region i (Ru atoms 1a, 4a and 5a, Figure 8), such kind of adsorption is not stable, and the CO_{ad} molecule relaxes spontaneously to adsorption on a Ru edge atom in the middle layer (Ru 5a, -2.48 eV). The situation is different for adsorption in region ii (Ru atoms 2a, 3a and 6a), where CO can adsorb on a bridge site (Ru atoms 2a and 6a). The adsorption energy of -1.82 eV (Figure 9) is, however, significantly smaller than in the previous cases. Overall, this means that for a Ru/ZrO_2 catalyst CO adsorption on the Ru atoms in the second layer above the interface is most stable, and these sites will be populated first, followed by adsorption on edge/surface atoms in higher layers, which for realistic nanoparticle sizes are the by far dominant number of sites. The tendency of CO to bind more strongly to the Ru atoms in the middle layer than to atoms in the interface layer can be explained by bond order effects. The strong interaction between metal atoms in the interface layer of the nanorod and the substrate can lead to a weaker interaction with the next

metal layer, which increases their reactivity towards CO adsorption.[34] This may over-compensate effects cause by the more pronounced charging of the Ru atoms in the interface layer and structural effects, due to the close proximity to the support. In the end, both of them should of course be reflected in the LDOS of the binding Ru atoms close to the Fermi level.

In the presence of a single O-vacancy and for adsorption on the nanorod surface, the most favorable adsorption site changes from the top site to a bridge site (see Figure 6). The adsorption energy remains about constant at about -2.00 eV (see Figure 10a). Apparently, despite the very small change in charge density on this site (before adsorption) and also in adsorption energy compared to the pristine support, this is enough to induce a change in adsorption site. Adsorption on the middle layer edge atom leads to a slight increase of adsorption energy compared to $0V_O$ to -2.61 eV (on-top adsorption). For adsorption close to the interface, we find now stable adsorption in region i on a bridge site involving Ru atoms in the middle layer (5a site) and in the interface layer (1a site), respectively. The adsorption energy of -2.62 eV is very close to that for adsorption on the middle layer Ru atom 5a, indicating that the additional interaction with the Ru bottom atom,1a and the neighboring Zr ion (Zr – O distance 2.33 Å) and the tilt energy cancel out. Adsorption in region ii, on a bridge site formed by Ru atoms 2a and 6a and involving also bonding interactions to a neighboring Zr (Zr – O distance 2.45 Å), is less favorable than in region i (adsorption energy -1.93 eV), which may be related to the relatively long distance between the Ru atom 2a and the O-vacancy. The higher adsorption energy in region i goes along with a higher charging of the Ru atoms in region i compared to those in region ii. Furthermore, we expect a direct interaction between Ru (Ru 1a) and the most reduced Zr^{n+} ion (3Zr), based on their short distance. From the same reason we expect a bonding interaction between the less reduced Zr^{n+} ion (2Zr) and the O-atom of the CO molecule adsorbed in region I, while it is slightly longer for CO adsorbed in region ii. This goes along with a significant increase of the CO adsorption energy compared to the $0V_O$ system, reaching -2.62

eV (see Figure 7). Obviously, the influence of the O-vacancy depends strongly on its distance to the adsorption site. Overall, also in this case, adsorption on a Ru atom in the second ('middle') layer is most favorable.

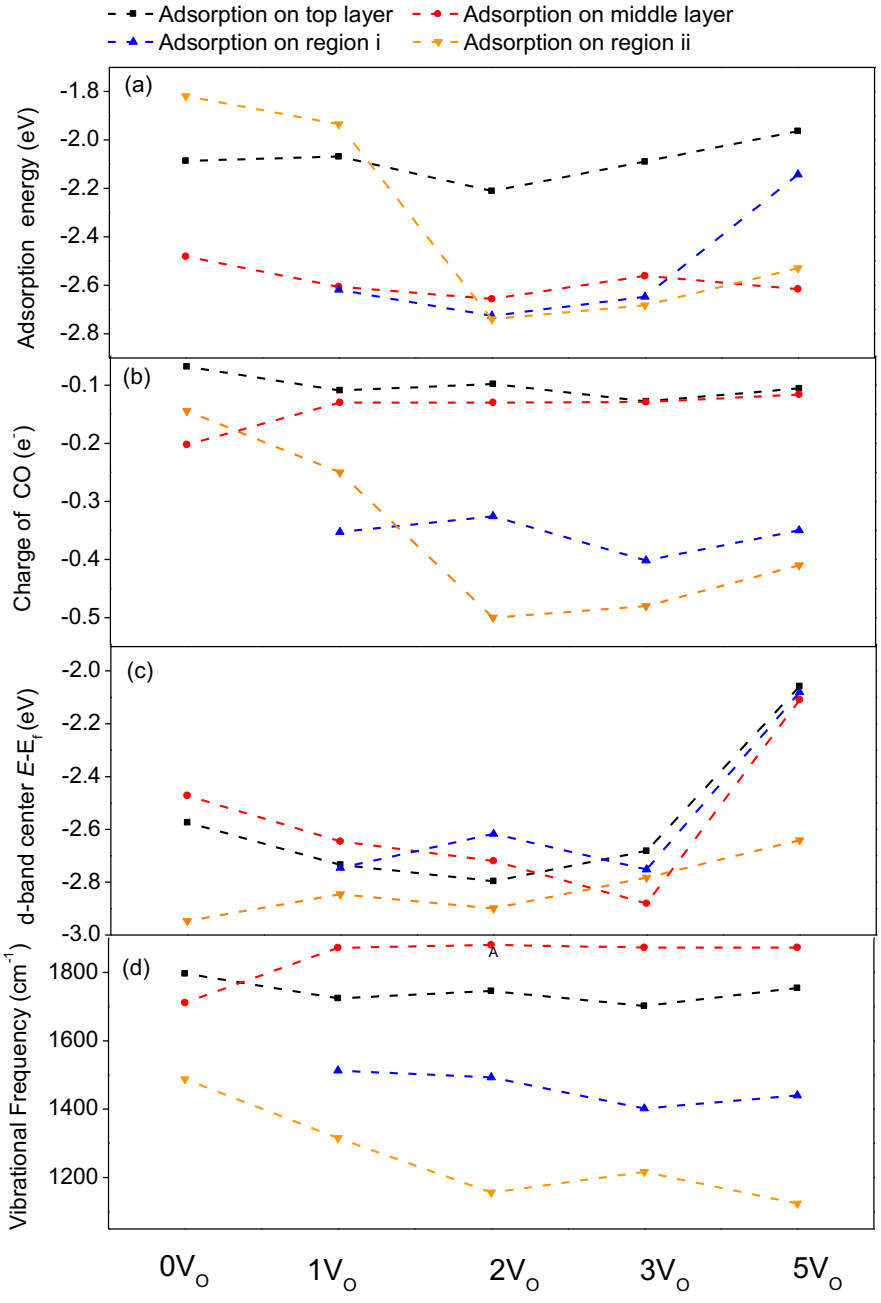

Figure 10 Variation of a) the adsorption energy, of b) the total charge transfer to CO, of c) the position of the d-band center of the Ru atoms involved in CO binding and of d) the vibrational frequency of CO adsorbed on the four different adsorption sites as f(O-vacancies).

In the presence of two O-vacancies, adsorption at the nanorod surface preferentially occurs at a bridge site (Ru atoms 7a and 8a, see Figure 6). In this case, there is also a slight increase of the adsorption energy to -2.21 eV (Figure 6). The adsorption energy at the middle layer remains around -2.60 eV (top site adsorption, Figure 7). For adsorption close to the interface, we again find stable adsorption both in region i and region ii, with rather similar adsorption energies of -2.73 and -2.74 eV, respectively. In region i, CO adsorbs on a hollow site created by two Ru atoms in the middle layer (1a and 4a) and one Ru atom (5a) in the interface layer (Figure 8). As before there is a binding interaction between the O atom of CO and an adjacent Zr^{n+} ion (Zr – O distance 2.30 Å, vs 2.55 Å in the absence of O-vacancies). In region ii, CO also adsorbs on a hollow site, involving two Ru sites (2a, 3a) in the bottom layer and one Ru atom in the middle layer (6a) (Figure 9), and again we expect some binding interaction with an adjacent Zr^{n+} ion (Zr – O distance 2.16 Å). The similar adsorption energies obtained for adsorption in regions i and ii mainly result from the fact that in this case each of the adsorption sites has an O-vacancy closely neighbored. At this charge concentration, CO adsorption at the interface becomes at least equally stable as that at the middle layer, indicating that Ru charging effects become comparable to structural and simple bond order effects.

Comparable results are obtained also for CO adsorption on the Ru nanorod with three O-vacancies underneath, both with respect to the adsorption energies and with respect to the preferential adsorption sites.

Finally, for five O-vacancies and adsorption at the Ru nanorod surface, we find preferential adsorption on a bridge site, with an adsorption energy slightly lower than obtained for lower numbers of O-vacancies (-1.96 eV, Figure 6). The adsorption energy on the middle layer of the Ru nanorod remains around -2.60 eV, with the same on-top adsorption site (Ru 5a, Figure 7). The situation is different for adsorption at the interface sites (Figures 8, 9), where the adsorption energies decrease to -2.14 eV (region i) and -2.53 eV (region ii), while the adsorption sites

remain the same as in the case of three O-vacancies. Hence, in this case adsorption on the second ('middle') layer is again slightly more stable than adsorption closer to the interface (in region ii), indicating that with the higher number of O-vacancies Ru charging effects again overcompensate structural and simple bond order effects.

In a first step to better understand the CO adsorption strength we split the interaction with the Ru atoms binding to the adsorbing CO into two different contributions, the energy required for deformation of the catalyst in the process of CO adsorption (deformation energy E_{cata}^{deform}) and the binding energy between the deformed catalyst and gaseous CO ($E_{cata\text{-}CO}^{bind}$). Here the catalyst deformation energy was calculated from the energy difference of the bare $Ru/ZrO_{2-x}(111)$ catalyst in its stable structure (without adsorbed CO) and in the structure obtained after CO adsorption. This shows (see Figure S2) that the contributions of $E_{cata\text{-}CO}^{bind}$ and also the changes therein are much larger than those of the deformation energies E_{cata}^{deform}, indicating that the formation of the Ru-CO bond dominates the changes in the CO adsorption energy with increasing number of O vacancies, while catalyst deformation plays only a minor role.

To gain more information about the interaction between metal and CO, we evaluated the charge transfer to the adsorbed CO in a next step. According to the Blyholder scheme,[35] CO adsorption is based on two contributions: i) electron donation from the CO-5σ orbital to the Ru-d states (CO-5σ → Ru-4d) and ii) back-donation from Ru-d states to the CO-2π* orbital (Ru-4d → CO-2π*). Since the 5σ orbital is located well below the Fermi level, the Ru – CO interaction is dominated by the interaction of the Ru-4d → CO-2π* states. In that case, the electron transfer from the Ru nanorod to the adsorbing CO will be decisive for the Ru-CO interaction. Therefore we determined the effective electron transfer to the adsorbed CO, by comparing the CO charge before and after CO adsorption. The charge transfers resulting for CO adsorption on the different sites, on the top layer, on the middle layer, and close to the interface in regions i and

ii, respectively, are summarized in Figure 10b for an increasing number of O-vacancies. The data clearly resolve very different trends in the charge transport behavior. For CO adsorption on the top layer (black line) and middle layer (red line) sites the charge transfer to CO is rather small, mostly around -0.1 e, and does not change much for an increasing number of O-vacancies. Only for the fully oxidized support ($0V_O$), the charge transfer is smaller for CO on the on-top site and larger on the middle-layer site. In contrast, for CO adsorption close to the interface, in regions i and ii, the charge transfer is significantly larger and for adsorption in the region ii, it varies strongly with increasing number of O-vacancies. While for adsorption in region i, the charge transfer is around -0.3 e, independent of the number of O-vacancies (blue line), adsorption on region ii (orange symbols / line) leads to a small charge transfer for $0V_O$, which increases up to -0.5 e for $2V_O$, and then decays slightly to about –0.4 eV for $5V_O$. In general, the trends in the charge transfer closely follow those in the CO adsorption energy, with one exception. While the charge transfer to CO is approximately identical for adsorption on the top-layer and middle layer sites, the adsorption energies differ significantly, with adsorption on the middle layer sites being significantly stronger. Thus, charge transfer to the CO is not the only effect determining the binding strength of the adsorbed CO.

Alternatively, trends in adsorption energies and for CO adsorption in particular are often described in terms of the d-band model.[18] which relates the adsorption energy of an adsorbate on a specific metal to the position of the center of the d-band on the respective adsorption site. An upward shift of the center of the d-band typically leads to an increased adsorption energy. Consequently, we evaluated the energy positions of the center of the Ru 4d-band on the different adsorption sites for an increasing number of O-vacancies. The resulting trends are plotted in Figure 10c. In general, there is much less agreement between the trends in the d-band center and in the adsorption energy than for charge transfer and adsorption energy. E.g., for adsorption on top-layer (black line) and middle-layer (red line) sites, the d-band center shifts to

significantly higher energy, while the adsorption energy remains almost constant. Also, there is little difference in the d-band center energy for these sites, while the adsorption energies differ significantly. For adsorption on the interface region i (blue line), we find a pronounced discrepancy in trends when going from $3V_O$ to $5V_O$, where the d-band center shifts closer to the Fermi level, while the adsorption energy decreases significantly. For lower number of O-vacancies, the trends in these properties are comparable (no significant change with number of O-vacancies), but on an absolute level the energy of the d-band center is close to that of the top-layer adsorption site, while the adsorption energies differ significantly. Finally, the pronounced increase of the adsorption energy for adsorption on the region ii with increasing number of O-vacancies goes along with only small up-shifts of the d-band center. Overall, the position of the d-band does not seem to be a good descriptor for trends in the adsorption energy in this system, and other effects need to be considered as well. Here it should be noted that there are also other systems in which the adsorption energies do not follow the trends predicted by the d-band model.[36;37]

Finally, we also calculated the vibrational frequency of the adsorbed CO (see Figure 10d). While absolute values of frequencies derived from DFT calculations often have to be taken with caution, trends in the calculated frequencies herein are generally considered to be reliable.[38] For adsorption on top-layer sites (black line), the frequency closely follows the trend of the charge transfer, with slightly lower vibrational frequencies for increasing (negative) charge transfer to adsorbed CO. This fully agrees with expectations based on the Blyholder picture for stronger back-donation from the metal to the adsorbed CO. For adsorption on middle-layer sites (red line), the trends also seem to agree rather well. For adsorption on the interface region i (blue line), the generally lower vibrational frequency as compared to the previous sites agrees well the larger charge transfer to adsorbed CO, from $1V_O$ to $5V_O$, and also the trends (no significant changes) agree well. Finally, for adsorption on interface sites in region ii (orange line), where

the changes with increasing number of O-vacancies were most pronounced, we find reasonable agreement between frequency shifts and charge transfer for the lower number of O-vacancies, where increasing (negative) charge transfer goes along with decreasing vibrational frequency, as expected for stronger back-bonding. This seems to be different for the $5V_O$ system, where decreasing charge transfer goes along with a decay in vibrational frequency, though the overall changes are rather small compared to $3V_O$, both for charge transfer and vibrational frequency. Overall, the trends in the C-O vibrational frequencies agree reasonably well with those in the charge transfer to adsorbed CO, as expected in the Blyholder model if charge transfer is dominated by transfer to the $2\pi^*$ state of CO, while there are discrepancies compared to the trends in the CO adsorption energy. Interestingly, changes in the C-O vibrational frequency do not always correlate well with changes in the CO adsorption energy, as it is often assumed, although in many cases these trends agree quite well.

In summary, we find a general trend that CO adsorption is much stronger for adsorption at the middle layer Ru atoms than on the surface of the Ru nanorod (top-layer sites). For adsorption close to the interface, in regions i and ii, this depends on the number / concentration of O vacancies. Furthermore, for CO adsorption on top-layer sites and at the middle layer of the Ru nanorod the adsorption energy varies only little with increasing number (concentration) of O-vacancies at the interface, underneath the Ru nanorod. This is different for CO adsorption at Ru atoms close to the interface, in regions i and ii, where the adsorption energy is either initially almost constant and then decreases (region i) or first increases and then decreases again (region ii) with increasing number of O-vacancies. Comparing the trends in CO adsorption energy with those in the three characteristic properties charge transfer to CO, d-band position of the metal atoms acting as adsorption site, and C-O frequency of adsorbed CO, we find that these can give a reasonable description of part of the trends in the adsorption energy, but fail to provide a complete picture, even on a qualitative scale. Among these properties, the energy of the center

of the d-band turned out to show the strongest deviations from the trends in CO adsorption energy as a function of the O-vacancy concentration. The sequence of adsorption energies was mainly explained by a competition between bond order effects, favoring adsorption at the second ('middle') layer, and charge transfer effects, which can stabilize adsorption more closely to the interface, both of which are reflected also in the LDOS of the binding Ru atoms in the region below the Fermi level (see also section 3.3). Charge transfer and charge transfer effects depend strongly on the distance between the Ru atoms binding to CO and the interface (vertical separation) and also to the closest vacancy (vertical and lateral separation). Thus, the influence of the O-vacancies on the CO adsorption characteristics is essentially confined to CO adsorption close to the interface (regions i and ii), which agrees well with the highly localized electron transfer from the support to the interface (bottom) layer of the Ru nanorod. In this case also interactions between the O atom of CO and a neighboring Zr^{n+} ion can play a role, based on the short bond distance. Finally, even very small changes in the adsorption energy may result, however, in a change in the preferential adsorption site.

3.3 Synergistic effect of support and Ru bottom layer

For a more detailed understanding of the role of the support for the interaction with adsorbed CO and of possible synergistic effects therein, we tried to separate different contributions to CO binding and charge transfer to/from adsorbing CO. As illustrated in Figure 11, these include interactions of Ru edge atoms in the different layers of the Ru nanorod and of the Zr^{n+} ions with the adsorbed CO, and charge transfer from these species to/from the adsorbed CO. For charge transfer from the Zr^{n+} surface species, this includes direct and indirect contributions, charge transfer directly to the adsorbed CO and charge transfer via the Ru nanorod. In addition, there may be a change in the ZrO_{2-x} and Ru interaction and a related charge transfer induced by adsorbing CO. Since we cannot separate such CO adsorption induced charge transfer from the support ZrO_{2-x} via the Ru nanorod to CO from charge transfer to the Ru nanorod and, decoupled

from that, charge transfer from the Ru nanorod to the adsorbed CO, the latter is essentially included in the direct charge transfer from the support to the adsorbed CO.

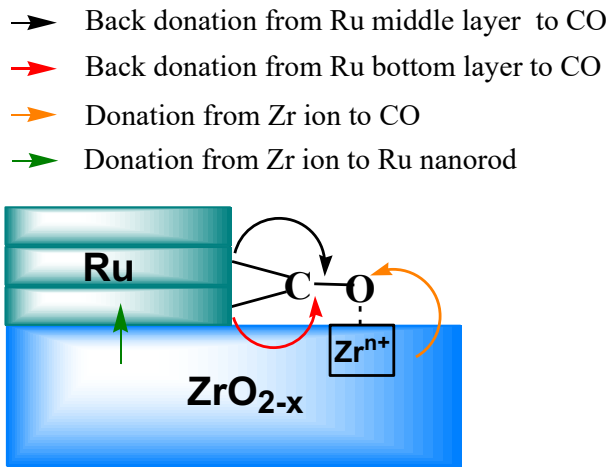

Figure 11 Schematic representation of the different contributions to the electron transfer to CO and to the adsorption energy for CO adsorbed on the different CO adsorption sites of the Ru/ZrO_{2-x}(111) model catalyst (see Figures 7 – 10).

The different contributions to the charge transfer from the catalyst to the adsorbed CO are plotted in Figure 12 as a function of an increasing number of O vacancies for the different adsorption sites. Note that the total charge transfer to CO was shown already in Figure 10b. The different trends can be summarized as follows. For CO adsorbed on a top-layer site (Figure 12a), the electron transfer from the Ru nanorod dominates (green and orange symbols / lines). Interestingly, for the fully oxidized support ($0V_O$), most of the electron transfer stems from Ru atoms which do not bind to CO directly (green symbols / line), such as the slightly negatively charged Ru 8a site. (Note that these charges refer to the charge state of the Ru atom before CO adsorption.) Hence, in this case the charge transfer is mediated via the neutral Ru 7a adsorption site. In the presence of O-vacancies, electron transfer mostly comes from Ru atoms binding to CO directly, in this case from the slightly negatively charged Ru 7a and 8a atoms.

For CO adsorbed on middle-layer sites, contributions from charge transfer from the support are significantly larger (blue symbols / line), and this increases with increasing number of O-

vacancies. But still, charge transfer is dominated by transfer from the Ru nanorod. In this case, charge comes mainly from Ru atoms not binding directly to CO, rather than from the slightly

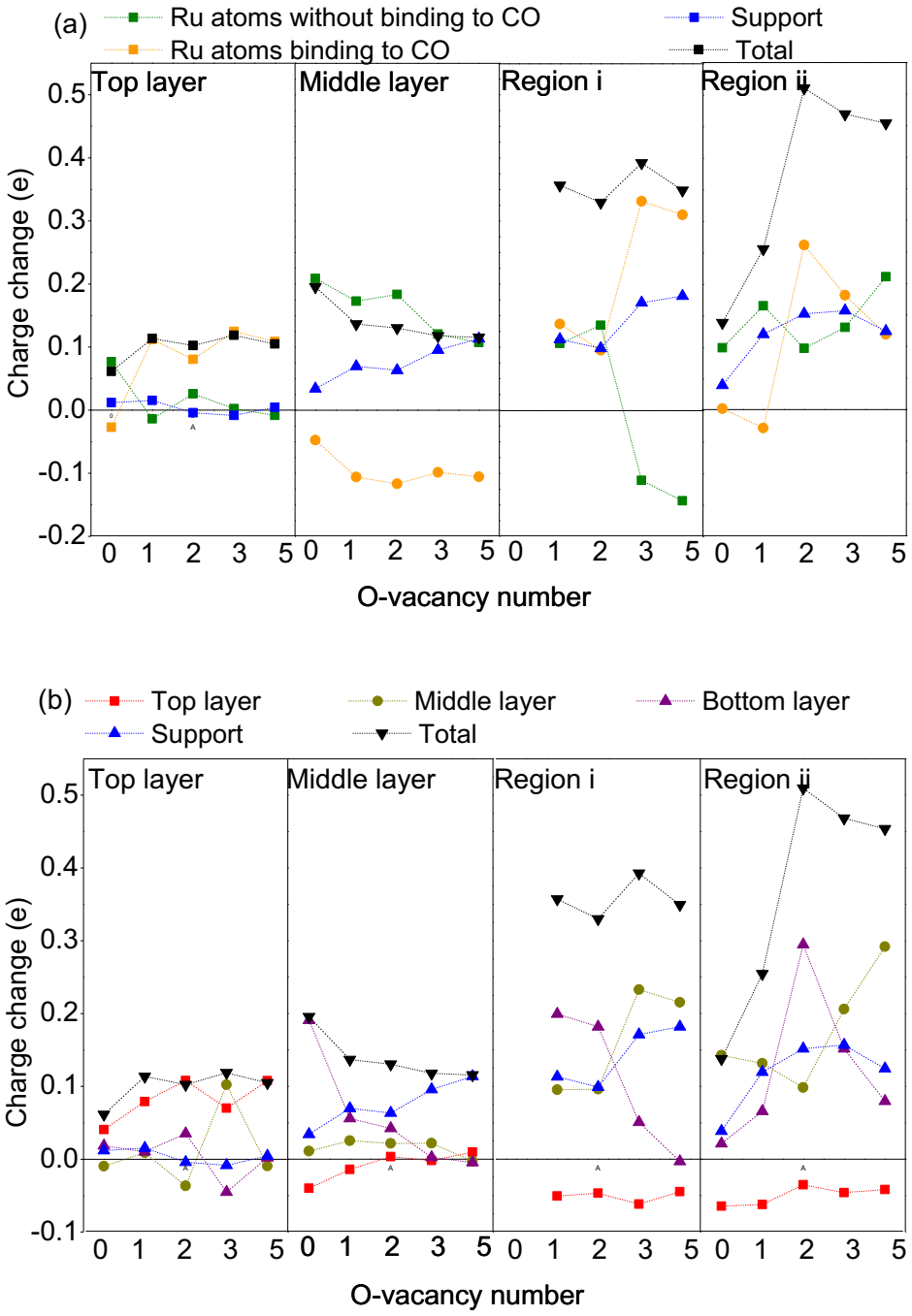

Figure 12. a) Charge transfer from the Ru atoms forming the CO adsorption sites to CO, from the remaining Ru atoms to CO and from the support to CO as f(O-vacancies). b) Charge transfer from the top, middle and bottom layers in the Ru nanorod and from the support to CO adsorbed on the top layer, middle layer, and in regions i and ii) as f(O-vacancies). Here CO adsorption induced charge transfer from the support ZrO_{2-x} via the Ru nanorod to CO is essentially included in the direct charge transfer from the support to CO.

positively Ru 5a adsorption site. Because of the still rather long distance between support and CO, we expect that the charge transfer from the support to the adsorbed CO mostly results from indirect charge transfer, via the Ru nanorod. The situation becomes more complex for adsorption in the interface regions i and ii. In both cases, the relative and also absolute amount of charge transfer from the support increases again. For CO adsorbed on interface region i, electrons are transferred with about equal fractions from the Ru atoms directly binding to CO, from the other Ru atoms and from the support. For higher numbers of O-vacancies, $3V_O$ and $5V_O$, the total charge transfer increases significantly, coming mostly from Ru atoms directly involved in CO binding, in particular from the Ru atom 1a, but also from the support. For CO adsorbed in region ii, where electron transfer to CO is most pronounced, transfer from the support first increases from $0V_O$ to $2V_O$, and then decreases again to $5V_O$. But also in this case, electron transfer to CO comes mostly from the Ru nanorod. For low O-vacancy concentrations it predominantly stems from atoms not binding directly to CO adsorption site, while for higher concentrations ($2V_O$ and higher) charge transfer from the adsorption site dominates. Thus, for all adsorption sites we find that charge transfer from the Ru nanorod does not only originate from Ru adsorption sites but also from more distant Ru atoms, illustrating the non-local effects for adsorption on a metal.

A comparable formal analysis of the charge transfer, but in this case distinguishing between charge contributions from the different layers of the Ru nanorod (Figure 12b), results in the following trends: For CO adsorbed at the top layer, most of the charge transfer comes from the top-layer Ru atoms (red symbols / line), independent of the number of O-vacancies, and contributions from the other two layers are small. The trend of constant charge transfer, which for all O-vacancy concentrations comes mostly from the Ru adsorption site, correlates well with the negligible changes in CO adsorption energy for this site. For adsorption at the middle layer (red symbols / line), the trend is different. Here, most electrons are transferred from the support

and from the bottom layer, mainly from the 1a and 2a sites with their higher charge density, and the charge on the Ru atoms in the top layer increases, while changes in the middle layer (Ru 4a, 5a, 6a) are small and have cancelled out. The slow decrease in the total charge transfer is first ($0V_O$ - $1V_O$) dominated by the decreasing charge transfer from the Ru bottom layer (purple symbols / line), while the other contributions increase slightly or change little (transfer from the middle layer). For increasing O-vacancy formation ($2V_O$ - $5V_O$), there is almost no charge transfer from the middle and top layer Ru atoms, while that from the support increases significantly, almost compensating the further decreasing charge transfer from the Ru bottom layer. In this case, the trend of little changes in the CO adsorption energy fits best to the trend in total charge transfer, while effects from the more pronounced changes in the individual contributions are less obvious. Overall, we find that electron transfer from more distant Ru atoms comes mostly from Ru atoms neighboring to O-vacancies. Finally, the compensating charge transfer contributions from support and bottom seem to be responsible for the almost constant CO adsorption energy.

For adsorption on interface region i, charge is mainly transferred from the Ru atoms in the middle and bottom layers and from the support to the adsorbed CO, while for Ru atoms in the top layer CO adsorption results in an increase of negative charge (negative charge transfer). With increasing O-vacancies ($1V_O$, $2V_O$) the bottom Ru layer, specifically the Ru atoms 1a and 2a, contribute more to the electron transfer than those of the support and middle layer. After the third O-vacancy formation, more electrons are transferred from the middle layer, specifically from the Ru 4a and 5a atoms, than from the support and the bottom layer, with the last contribution decreasing almost to zero. The change of the dominant contribution, from bottom layer to middle layer, agrees well the increasing electron density of the middle layer sites (Ru 4a, Ru 5a) and the decreasing electron density of the Ru 1a and Ru 2a sites in the bottom layer (Table 2). Finally, despite of the more pronounced charge transfer from the middle layer Ru

atoms to CO at the third O-vacancy formation, the adsorption energy decreases, most likely due to the significant decrease of the total charge transfer to CO.

Finally, for adsorption on interface region ii, where the change in total charge transfer to CO is most pronounced, this first increases strongly from $0V_O$ to $2V_O$ and then decreases. This agrees well with the opposite trend of the CO adsorption energy (Figure 10a). The trend in the total charge transfer is first ($0V_O$ - $2V_O$) dominated by charge transfer from the Ru bottom layer, which is higher than that from the support, while the other contributions change little. For further increasing O-vacancy formation ($3V_O$ - $5V_O$), charge transfer from the middle layer rapidly increases, while the total charge transfer and in particular that from the bottom layer decrease.

As a last step, we also calculated the local density of states (LDOS) for the 4d-states at the Ru atoms binding to adsorbed CO and of the 5σ and 2π* orbitals of the adsorbed CO molecule for the different CO adsorption sites as a function of the number of O vacancies. These calculations well confirmed Blyholder's donation-backdonation model in agreement with previous calculations [39]: in all cases, there is a 5σ derived LDOS at the CO molecule above the Fermi energy, indicating electron donation to the Ru atoms, but also a 2π* derived LDOS below the Fermi energy confirming the electron backdonation. However, the differences in the LDOS as a function of the number of vacancies at the different considered adsorption sites are not significant enough to derive any new insights that go beyond those already discussed above.

3.4 Correlations between different effects induced by O-vacancies and implications

The results presented and discussed in the previous sections have provided a detailed picture of the way how the presence of O-vacancies at the interface to a metal nanoparticle, in this case of a Ru nanorod, can modify the CO adsorption properties and thus also the catalytic performance of Ru/ZrO_2 catalysts. In a more general picture, we expect similar trends also for

other oxide supported metal nanoparticle catalysts. Charge transfer from the O-vacancy to these metal atoms results in a modified population of $2\pi^*$ orbitals of the adsorbed CO, leading to a change in adsorption energy and in the frequency of internal vibrations of the adsorbed molecules. The fact that significant effects are only observed for O-vacancies close to the adsorbate-carrying Ru atom, i.e., for CO adsorption close to the interface, means that such effects are dominated by O-vacancies close to the perimeter of the metal nanoparticles. Deeper-lying O vacancies or O-vacancies further away from the metal nanoparticle edge, both outside the metal nanoparticle and more inside underneath the metal nanoparticles, can essentially be neglected in the evaluation of electronic metal-support interactions. On the other hand, this also means that for nanoparticles of sizes exceeding a few nanometers, EMSIs will affect only a small amount of the metal surface atoms, namely those at the interface perimeter of the nanoparticles, in contrast to a 'charge transfer to the (entire) metal nanoparticle', as it is often stated in the literature. Therefore, spectroscopic measurements testing all adsorption sites, as, e.g., in *in situ* DRIFTS measurements performed at close to saturation coverage, will hardly resolve species adsorbed on these sites. On the other hand, for weakly adsorbing reactants, only such sites may be populated under reaction conditions, which allows a facile identification of the species. Examples are supported Au catalysts, where the (sole) observation of CO_{ad} species with vibrations well below 2100 cm^{-1} was reported,[14] which are characteristic for CO adsorption on negatively charged Au sites / clusters.[6;40] Preferential adsorption on perimeter sites of 2D Au aggregates on a MgO film was even observed directly by scanning tunneling microscopy.[41] Furthermore, gradually increasing charge transfer to the entire nanoparticle, i.e., to more or less all surface sites of the metal nanoparticle, would result in a continuous change in the charge of the surface sites. For adsorbed CO as a molecular probe this would result in a continuous shift of the C-O vibrational frequency, in contrast to experimental observations, which reported co-

existence of two bands typical for CO on essentially neutral sites and CO adsorbed on negatively charged metal sites, e.g., for CO adsorbed on Au/TiO_2 catalysts.[6]

When considering the relevance of the present work for realistic supported catalysts and catalytic reactions one has to keep in mind that in most cases the active metal nanoparticles exhibit a multitude of different sites, which due to their different distance to the interface will be differently affected by the presence of O-vacancies at the interface. For nanoparticles with sizes exceeding a few nanometers this means that many if not most sites will essentially not be affected by the formation of O-vacancies, at least not measurably. Nevertheless, the formation of O-vacancies will allow to modify the adsorption energies on this fraction of available surface sites. Since according to the Sabatier principle [33] there is a correlation between the activity of the active sites and the adsorption energy of the adsorbed species (reactants, intermediates, products), this will modify also the catalytic activity of these sites. In the extreme case, these sites close to the interface represent the active sites, which despite of their low abundance dominate the catalytic performance. In this case it would be hardly possible to spectroscopically identify these active sites because of their low number. This also means that it should be possible to tune and optimize the performance of a catalyst by proper optimization of the reductive character of the reaction gas mixture or of the reducibility of the catalyst support, e.g., by doping.[42]

Equally important for the charge transfer is also the surface structure of the support material. Here we expect rather different results in the charge transfer for different polar surfaces of the same material, and hence in the electronic modification of the interface metal atoms, depending on the surface termination. For non-polar support surfaces like the $ZrO_2(111)$ surface investigated here, the charge transfer and thus the electronic modification of the interface metal atoms will still vary laterally, albeit with a lesser extent, depending on whether the respective interface metal atom is closer to a metal cation or to an O^{2-} anion. Nevertheless, it should still

be possible to predict general trends in charge transfer, considering also the stability of different surface and interface orientations.

Finally, one should also keep in mind that interface vacancy formation may not only affect the activity of a catalyst by electronic metal-support interactions (EMSIs), as illustrated in the present case, but may also be part of the reaction cycle itself, where formation of vacancies provides active oxygen. This is well known for the Mars – van Krevelen reaction mechanism.[43] Similar effects have been demonstrated previously, however, also for a number of reactions over Au catalysts supported on reducible oxide supports, where continuous formation and depletion of surface vacancies at the perimeter of Au nanoparticles ('Au-assisted Mars-van Krevelen mechanism') is part of the reaction cycle.[12;13;16]

4 Conclusions

Based on systematic DFT calculations we have comprehensively investigated the effect of an increasing number of O-vacancies at the interface between a reducible oxide and a metal nanoparticle, modelled by a ZrO_2(111) support and a Ru nanorod, on the adsorption of CO. We demonstrated that the effect of an O-vacancy on the chemisorption behavior of Ru surface atoms is highly localized, both laterally and vertically, and mainly affects Ru atoms at the Ru-ZrO_{2-x} interface directly neighbored to the vacancy. For an increasing number of O-vacancies underneath the Ru nanorod, the changes in adsorption energy are negligible for adsorption on the surface of the 3-layer nanorod. Similar results are obtained also for adsorption at the second layer above the interface, which is also significantly more stable than that on higher layers. Pronounced variations with increasing number of O-vacancies are obtained only for CO adsorption energy on Ru interface sites, which can even make adsorption on these sites most stable. We gave a detailed picture of the O-vacancy induced changes in the bonding situation, both of the Ru nanorod ('metal - support interactions') and of adsorbed CO. This includes

changes in the charge of the Ru nanorod upon interaction with the support and of the CO upon adsorption at different sites on the Ru/ZrO_{2-x}(111) model system, both as far as changes in the total charge and locally resolved changes are concerned, which reflect CO adsorption induced charge transfer from the support to the Ru nanorod and from both Ru and the support to the adsorbed CO molecule. As a further parameter, we also calculated the C-O vibrational densities on different adsorption sites and O-vacancy induced changes therein, and correlated these with the trends in charge state and in adsorption energy. The trends in the adsorption energy are rationalized by changes in the LDOS, which were calculated for the different adsorption sites and for the adsorbed CO molecule. Finally, we outlined effects of O-vacancies on the adsorption and catalytic properties of realistic, oxide supported metal nanoparticle catalyst, and proposed the systematic optimization of electronic metal-support interactions by O-vacancy generation, e.g., by tuning the oxidative character of the reaction gas or by modifying the reducibility of the support, as an interesting strategy for improving the performance of these catalysts.

Acknowledgements

We acknowledge computer time provided by the state of Baden-Württemberg through the bwHPC program and the German Research Foundation (DFG) through grant INST 40/575-1 FUGG (JUSTUS II cluster). Furthermore, we would like to thank Sung Sakong for fruitful discussions.

References

1. Tauster, S. J.; Fung, S. C.; Garten, R. L. Strong Metal-Support Interactions. Group 8 Noble Metals Supported on TiO_2, *J. Am. Chem. Soc.* **1978**, *100*, 170-175.

2. Tauster, S. J.; Fung, S. C.; Baker, R. T. K.; Horsley, J. A. Strong Interactions in Supported-Metal Catalysts, *Science* **1981**, *211*, 1121-1125.

3. Campbell, C. T. Catalyst-Support Interactions: Electronic Perturbations, *Nat. Chem.* **2012**, *4*, 597-598.

4. Ahmadi, M.; Mistry, H.; Roldan Cuenya, B. Tailoring the Catalytic Properties of Metal Nanoparticles Via Support Interactions, *J. Phys. Chem. Lett.* **2016**, *7*, 3519-3533.

5. van Deelen, T. W.; Hernandez Mejia, C.; de Jong, K. P. Control of Metal-Support Interactions in Heterogeneous Catalysts to Enhance Activity and Selectivity, *Nat. Catal.* **2019**, *2*, 955-970.

6. Pacchioni, G.; Freund, H. J. Controlling the Charge State of Supported Nanoparticles in Catalysis: Lessons From Model Systems, *Chem. Soc. Rev.* **2018**, *47*, 8474-8502.

7. Sicolo, S.; Giordano, L.; Pacchioni, G. CO Adsorption on One-, Two-, and Three-Dimensional Au Clusters Supported on MgO/Ag(001) Ultrathin Films, *The Journal of Physical Chemistry C* **2009**, *113*, 10256-10263.

8. Sawabe, K.; Satsuma, A. Theoretical Study on Carbon Monoxide Adsorption on Unsupported and +¦-Al2O3-Supported Silver Nanoparticles: Size, Shape, and Support Effects, *ACS Omega* **2022**, *7*, 4405-4412.

9. Chen, S.; Abdel-Mageed, A. M.; Li, M.; Cisneros, S.; Bansmann, J.; Rabeah, J.; Brückner, A.; Groß, A.; Behm, R. J. Electronic Metal-Support Interactions and Their Promotional Effect on CO_2 Methanation on Ru/ZrO_2 Catalysts, *J. Catal.* **2021**, *400*, 407-420.

10. Abdel-Mageed, A. M.; Klyushin, A. Y.; Knop-Gericke, A.; Schlögl, R.; Behm, R. J. Negative Charging of Au Nanoparticles During Methanol Synthesis From CO_2 / H_2 on a Au/ZnO Catalyst: Insights From Operando Infrared and Near-Ambient Pressure XPS and XAS, *Angew. Chem. Int. Ed.* **2019**, *58*, 10325-10329.

11. Abdel-Mageed, A. M.; Klyushin, A.; Knop-Gericke, A.; Schlögl, R.; Behm, R. J. Influence of CO on the Activation, O-Vacancy Formation, and Performance of Au/ZnO Catalysts in CO_2 Hydrogenation to Methanol, *J. Phys. Chem. Lett.* **2019**, *10*, 3645-3653.

12. Widmann, D.; Behm, R. J. Active Oxygen on a Au/TiO_2 Catalyst - Formation, Stability and CO Oxidation Activity, *Angew. Chem. Int. Ed.* **2011**, *50*, 10241-10245.

13. Widmann, D.; Behm, R. J. Activation of Molecular Oxygen and the Nature of the Active Oxygen Species for CO Oxidation on Oxide Supported Au Catalysts, *Acc. Chem. Res.* **2014**, *47*, 740-749.

14. Wang, Y.; Widmann, D.; Behm, R. J. Influence of TiO_2 Bulk Defects on CO Adsorption and CO Oxidation on Au/TiO_2: Electronic Metal-Support Interactions (EMSIs) in Supported Au Catalysts, *ACS Catal.* **2017**, *7*, 2339-2345.

15. Wang, Y.; Widmann, D.; Heenemann, M.; Diemant, T.; Biskupek, J.; Schlögl, R.; Behm, R. J. The Role of Electronic Metal-Support Interactions and Its Temperature Dependence: CO Adsorption and CO Oxidation on Au/TiO_2 Catalysts in the Presence of TiO_2 Bulk Defects, *J. Catal.* **2017**, *354*, 46-60.

16. Schlexer, P.; Widmann, D.; Behm, R. J.; Pacchioni, G. CO Oxidation on a Au/TiO_2 Nanoparticle Catalyst Via the Au-Assisted Mars-Van-Krevelen Mechanism, *ACS Catal.* **2018**, *8*, 6513-6525.

17. Schlexer, P.; Ruiz Puigdollers, A.; Pacchioni, G. Role of Metal/Oxide Interfaces in Enhancing the Local Oxide Reducibility, *Top. Catal.* **2018**, *61*, 1-10.

18. Hammer, B.; Nørskov, J. K. Theoretical Surface Science and Catalysis-Calculations and Concepts, *Adv. Catal.* **2000**, *45*, 71-129.

19. Kresse, G.; Hafner, J. Ab Initio Molecular-Dynamics Simulation of the Liquid Metal–Amorphous-Semiconductor Transition in Germanium, *Phys. Rev. B* **1994**, *49*, 14251-14269.

20. Kresse, G.; Furthmüller, J. Efficiency of Ab-Initio Total Energy Calculations for Metals and Semiconductors Using a Plane-Wave Basis Set, *Comp. Mat. Sci.* **1996**, *6*, 15-50.

21. Kresse, G.; Furthmüller, J. Efficient Iterative Schemes for Ab Initio Total-Energy Calculations Using a Plane-Wave Basis Set, *Phys. Rev. B* **1996**, *54*, 11169-11186.

22. Blöchl, P. E. Projector Augmented-Wave Method, *Phys. Rev. B* **1994**, *50*, 17953-17979.

23. Kresse, G.; Joubert, D. From Ultrasoft Pseudopotentials to the Projector Augmented-Wave Method, *Phys. Rev. B* **1999**, *59*, 1758-1775.

24. Perdew, J. P.; Burke, K.; Ernzerhof, M. Generalized Gradient Approximation Made Simple, *Phys. Rev. Lett.* **1996**, *77*, 3865-3868.

25. Dudarev, S. L.; Botton, G. A.; Savrasov, S. Y.; Humphreys, C. J.; Sutton, A. P. Electron-Energy-Loss Spectra and the Structural Stability of Nickel Oxide: An LSDA+U Study, *Phys. Rev. B* **1998**, *57*, 1505-1509.

26. Wang, L.; Maxisch, T.; Ceder, G. Oxidation Energies of Transition Metal Oxides Within the GGA+U Framework, *Phys. Rev. B* **2006**, *73*, 195107.

27. Tolba, S. A.; Allam, N. K. Computational Design of Novel Hydrogen-Doped, Oxygen-Deficient Monoclinic Zirconia With Excellent Optical Absorption and Electronic Properties, *Sci. Rep.* **2019**, *9*, 10159.

28. Grimme, S.; Ehrlich, S.; Goerigk, L. Effect of the Damping Function in Dispersion Corrected Density Functional Theory, *J. Comput. Chem.* **2011**, *32*, 1456-1465.

29. Monkhorst, H. J.; Pack, J. D. Special Points for Brillouin-Zone Integrations, *Phys. Rev. B* **1976**, *13*, 5188-5192.

30. Manz, T. A.; Limas, N. G. Introducing DDEC6 Atomic Population Analysis: Part 1. Charge Partitioning Theory and Methodology, *RSC Adv.* **2016**, *6*, 47771-47801.

31. Limas, N. G.; Manz, T. A. Introducing DDEC6 Atomic Population Analysis: Part 2. Computed Results for a Wide Range of Periodic and Nonperiodic Materials, *RSC Adv.* **2016**, *6*, 45727-45747.

32. Sakong, S.; Groß, A. The Electric Double Layer at Metal-Water Interfaces Revisited Based on a Charge Polarization Scheme, *The Journal of Chemical Physics* **2018**, *149*, 084705.

33. Sabatier, P. *La Catalyse en Chimie Organique*, Librairie Polytechnique Béranger: Paris, 1913.

34. Roudgar, A.; Groß, A. Local Reactivity of Supported Metal Clusters: Pd_n on Au(111), *Surf. Sci.* **2004**, *559*, L180-L186.

35. Blyholder, G. Molecular Orbital View of Chemisorbed Carbon Monoxide, *J. Phys. Chem.* **1964**, *68*, 2772-2778.

36. Sakong, S.; Groß, A. Dissociative Adsorption of Hydrogen on Strained Cu Surfaces, Surf. Sci. **2003**, 525, 107-118.

37. Groß, A. Tailoring the Reactivity of Bimetallic Overlayer and Surface Alloy Systems, J. Phys.: Condens. Matter **2009**, 21, 084205.

38. Merrick, J. P.; Moran, D.; Radom, L. An Evaluation of Harmonic Vibrational Frequency Scale Factors, The Journal of Physical Chemistry A **2007**, 111, 11683-11700.

39. Aizawa, H.; Tsuneyuki, S. First-Principles Study of CO Bonding to Pt(111): Validity of the Blyholder Model, Surf. Sci. **1998**, 399, L364-L370.

40. Sterrer, M.; Yulikov, M.; Fischbach, E.; Heyde, M.; Rust, H. P.; Pacchioni, G.; Risse, T.; Freund, H. J. Interaction of Gold Clusters With Color Centers on MgO(001) Films, *Angew. Chem. Int. Ed.* **2006**, *45*, 2630-2632.

41. Lin, X.; Yang, B.; Benia, H.-M.; Myrach, P.; Yulikov, M.; Aumer, A.; Brown, M. A.; Sterrer, M.; Bondaschurk, O.; Kieseritzky, E.; Rocker, J.; Risse, T.; Gao, H.-J.; Nilius, N.; Freund, H.-J. Charge-Mediated Adsorption Behavior of CO on MgO-Supported Au Clusters, *J. Am. Chem. Soc.* **2010**, *132*, 7745-7749.

42. Cisneros, S.; Chen, S.; Diemant, T.; Bansmann, J.; Abdel-Mageed, A. M.; Goepel, M.; Olesen, S. E.; Welter, E. S.; Parlinska-Wojtan, M.; Gläser, R.; Chorkendorff, I.; Behm, R. J. Effects of SiO_2-Doping on High-Surface-Area Ru/TiO_2 Catalysts for the Selective CO Methanation, *Appl. Catal. B* **2021**, *282*, 119483-119483-11.

43. Mars, P.; van Krevelen, D. W. Oxidations Carried Out by Means of Vanadium Oxide Catalysts, Chem. Engin. Sci. **1954**, 3, 41 Supplement-59 Supplement.

Table of Contents Graphics